Title	Determination of the number of RAD51 molecules in different human cell lines
Author(s)	Foertsch, Franziska; Kache, Tom; Drube, Sebastian; Biskup, Christoph; Nasheuer, Heinz-Peter; Melle, Christian
Publication Date	2019-11-15
Publication Information	Foertsch, Franziska, Kache, Tom, Drube, Sebastian, Biskup, Christoph, Nasheuer, Heinz Peter, & Melle, Christian. (2019). Determination of the number of RAD51 molecules in different human cell lines. Cell Cycle, 18(24), 3581-3588. doi: 10.1080/15384101.2019.1691802
Publisher	Taylor & Francis
Link to publisher's version	https://doi.org/10.1080/15384101.2019.1691802
Item record	http://hdl.handle.net/10379/15684
DOI	http://dx.doi.org/10.1080/15384101.2019.1691802

Determination of the number of RAD51 molecules in different human cell lines

Franziska Foertsch[a], Tom Kache[a], Sebastian Drube[b], Christoph Biskup[a], Heinz Peter Nasheuer[c], Christian Melle[a*]

[a]Biomolecular Photonics Group, [b]Institute of Immunology, Jena University Hospital, Jena, Germany; [c]Centre for Chromosome Biology, National University of Ireland Galway, Galway, Ireland

[*]contact: Christian.melle@med.uni-jena.de

Keywords: molecules per cell, DNA double-strand breaks, homologous recombination, RAD51, ectopic protein expression

ABSTRACT

Knowledge about precise numbers of specific molecules is necessary for understanding and verification of biological pathways. The RAD51 protein is central in the repair of DNA double-strand breaks (DSBs) by homologous recombination repair and understanding its role in cellular pathways is crucial to design mechanistic DNA repair models. Here, we determined the number of RAD51 molecules in several human cell lines including primary fibroblasts. We showed that between twenty to one-hundred thousand of RAD51 molecules are available per human cell that theoretically can be used for simultaneously loading at least thirty-seven DSBs. Interestingly, the amount of RAD molecules does not significantly change after the induction of DNA damage using bleomycin or γ-irradiation in cells but an accumulation of RAD51 on the chromatin occurs. Furthermore, we generated an EGFP-RAD51 fusion under the control of HSV thymidine kinase promoter sequences yielding moderate protein expression levels comparable to endogenously expressed RAD51. Initial characterizations suggest that these low levels of ectopically expressed RAD51 are compatible with cell cycle progression of human cells. Hence, we provide parameters for the quantitative understanding and modeling of RAD51-involving processes.

INTRODUCTION

To determinate values of biological entities, concentrations, or numbers is important to understand their biological function [1]. Cells have developed mechanisms to repair damaged DNA that have been induced by both exogenous and endogenous sources [2]. Proteins participating in these processes are tightly regulated by post-transcriptional modifications, cellular localization, and protein expression levels [3]. Knowledge about precise numbers of proteins involved in the DNA damage repair is necessary for modeling of cellular repair pathways. The evolutionary conserved RAD51 protein is central for the repair of DNA double-strand breaks (DSBs) by homologous recombination repair due to its capacity to exchange DNA strands between homologous partners. Thereby, RAD51 forms filaments on 3′-end single-stranded DNA (ssDNA) of DSBs using BRCA2 and RAD51 paralogs activity. Subsequently, the resulting nucleoprotein filament is able to invade in homologous sequences and induce recombination processes [4]. The function of RAD51 is analyzed by several biochemical, cell biological, and biophotonic approaches using purified RAD51 protein as well as plasmids expressing RAD51 [5-14].

In the present study, we calculated the number of RAD51 molecules in different human cell lines as well as primary human fibroblast and determined the abundance of RAD51 in the chromatin fraction of cells after induction of DNA damage. Furthermore, we generated a stable human cell line to ectopically express RAD51 at levels comparable to the amount of endogenous RAD51 and performed initial characterizations of the cell line.

RESULTS AND DISCUSSION

For the modeling of DNA repair pathways by biochemical *in vitro* assays or live-cell imaging approaches using fusion protein it is advantageous to know precise numbers of proteins involved in the DNA damage repair in a cell. There are already some quantitative data available regarding the number of molecules of DNA repair proteins per cell such as RAD52, RPA, and POT1 [15-17] but none have been published for RAD51 in human cells so far. Here, we determined as far as possible the precise number of RAD51 molecules in human cell lines (Fig. 1). To accurately measure these RAD51 numbers, we analyzed whole cell extracts of six human cell lines derived from cervical and breast

adenocarcinoma, colon and hepatocellular carcinoma as well as osteosarcoma and keratinocytes by western blotting. Moreover, we determined the RAD51 number in two primary human fibroblast cell lines derived from skin (BJ) and lung (Wi38) [18]. For estimation of endogenous number of RAD51 we used purified RAD51 to prepare standard curves (Fig. 1A) [11]. From these quantitative western blots we calculated that approx. 2 – 10 x 10^4 RAD51 molecules per cell are present in these human cell lines (Fig. 1B-I, summarized in table Fig. 1, panel J) suggesting there are comparable RAD51 levels in these cells. One thousand molecules of a common cellular protein in HeLa correspond to a concentration of approx. 1 nM [19]. Here, we determined that RAD51 occur in distinct cell lines in a concentration of approx. 10 – 40 nM, which is comparable but lower than previously found for human RPA, which was determined to have concentration of 200 nM in the nucleus and 36 nM in the cytosol [17].

Beside its capacity to bind double-stranded DNA (dsDNA), RAD51 is able to bind specifically ssDNA to form nucleoprotein filaments. Each RAD51 monomer binds three nucleotides of ssDNA, and six monomers generate one turn of a helical RAD51-ssDNA filament [20]. Human cells generate approx. 10 – 20 DSBs per day in response to replication stress and as a consequence of endogenous DNA damage [21]. As the average length of ssDNA accumulating during allelic recombination is approx. 2 – 4 kb on each side of the break [22], we estimate that theoretical on average at least 7 (HepG2) to 37 (Wi-38) DSBs can be simultaneously loaded with RAD51 molecules to perform strand exchanges at homologous sequences. The concentration of cellular RAD51 is regulated tightly to avoid uncontrolled recombination events [3]. Indeed, our findings presented here suggest that adequate amounts of RAD51 are available in these cells to perform all recombination repair processes in cells.

Since it is well known that RAD51 expression needs to be strictly controlled we wondered whether DNA damage induces a changed protein expression of RAD51. Therefore, we treated cells with a cytotoxic agent or ionizing radiation to induce both DNA single- and double-strand breaks. The applied amounts of the chemical bleomycin (12.5 µg/ml) and γ-irradiation (5 Gy) are sufficient to generate several DNA lesions per cell but allow cells to survive due to DNA repair as shown previously [11,23]. In the experiments presented here we demonstrate that the induction of DNA damage by bleomycin has no influence on the total expression levels of human RAD51 protein when analyzed whole cell extracts (Fig. 2A) which is in agreement with a previous study [24]. The treatment of HaCaT keratinocytes with

γ-irradiation as an independent way to induce cellular DNA damage did neither show a significant alteration in the number of RAD51 molecules per cell 5 h after irradiation and numbers of RAD51 molecules in control and treated cells were comparable (Fig. 2B). Comparison of the numbers of RAD51 in HaCaT cells treated with bleomycin or γ-irradiation showed also no significant differences (Fig. 2B). RAD51 localizes to nuclear repair foci in response to DNA damage. Repair of DSBs by HR is at the latest completed 8 h post-damage as analyzed by immunofluorescence-based microscopy experiments. Thereby, content of RAD51 containing repair foci is comparable to controls after this time [11,25]. To perform its functions RAD51 has to localize on chromatin. Hence, we additionally biochemically analyzed the chromatin-bound fraction of RAD51 of bleomycin-treated U2OS cells over time by immunoblots (Fig. 2D). In contrast to RAD51 numbers determined in whole U2OS cell extracts (Fig. 2C), there was a clearly increase in RAD51 molecules detectable in the chromatin fraction 5 h after DNA damage induction, which was statistically significant compared to chromatin fractions derived from untreated control cells. Twenty-four hours post-DNA damage, the number of chromatin-bound RAD51 was again comparable to controls. Therefore, DSB damage induces an accumulation of RAD51 on chromatin but does not change the expression of RAD51 protein. These results underline that it is important to analyze proteins in the cellular compartment where they act.

The amount of RAD51 molecules in cells seems to be tightly regulated as RAD51 numbers are in comparable level in multiple transformed and primary human cell lines. To assess the effect of increasing RAD51 number, we analyzed the occurrence of both endogenous and ectopically expressed RAD51 regarding their cellular localization. In contrast to endogenous RAD51 showing nuclear localization in part as foci at sites of DNA repair, ectopically over-expressed EGFP-RAD51 using a CMV promoter construct forms rod-shaped nuclear structures in cells even without otherwise induced DNA damage (Fig. 3A and 3B both top panels). As RAD51 is able to bind both dsDNA and ssDNA, the rod-shaped pattern might be dsDNA/EGFP-RAD51 filaments as previously described [6]. Therefore, we compared the expression levels of endogenous and ectopically expressed human RAD51 (Fig. 3C). The quantification yielded 2.9×10^4 RAD51 molecules per U2OS cells, which is consistent with our results presented above, whereas the apparent numbers for CMV-EGFP-RAD51 would be twice as high yielding 5.8×10^4 RAD51 molecules per U2OS cell. Taking into account the transfection efficiency of

only 3% in an average experiment for the expression of CMV-EGFP-RAD51 yields an estimated number of $1.9x10^6$ of RAD51 protein molecules per U2OS cell or an approximately 65-fold overexpression of ectopically expressed EGFP-RAD51 over endogenous RAD51. Our determined level of human RAD51 is a magnitude lower compared to the abundance of its regulator Rad54 in MES cells [26]. It seems that the abundance of RAD51 has to be strictly controlled to avoid unregulated binding to dsDNA resulting in the increase of undesired recombination possibility.

Reducing ectopic expression level of fusion proteins has been used to minimize impacts on cellular functions [27]. Thus, we created an EGFP-RAD51 fusion using HSV thymidine kinase (TK) instead of CMV promoter sequences yielding moderate protein expression levels and reduced artificial influences on cells (Fig. 3B lower panels and panel 3D). Using these stable cell lines we determined that endogenous RAD51 was expressed at a level of $7.9x10^4$ molecules per stable U2OS cell, which is higher than in the parental cell line whereas the ectopic expression of TK promoter regulated EGFP-RAD51 is about 50% of this level. Taking into account that only 40% of the stable cell line express EGFP-RAD51 yields that TK-EGFP-RAD51 is ectopically expressed at $1.6x10^4$ molecules per cell, which is below the level of endogenous RAD51 and the level of the parental cell line. Together endogenous plus ectopically express RAD51 would reach a level of $9.5x10^4$ RAD51 molecules per cell which is lower than the RAD51 expression level in the non-transformed human fibroblast cells Wi-38 and at the same level as BJ cells (Fig. 1J) and thus well in the tolerance of human cells but much lower than the CMV-EGFP-RAD51 expression levels. The distribution of U2OS cells transfected with CMV-EGFP-RAD51 was strongly altered compared with non-transfected control cells. Cells expressing CMV-EGFP-RAD51 mainly accumulated in G2 compare to control cells. In contrast, TK-EGFP-RAD51 expressing cells showed a cell cycle distribution comparable to controls (Fig. 3E). An accumulation in the G2 phase of cells overexpressing RAD51 is already described [28]. Thus, this initial characterization shows the ectopic expression levels of EGFP-RAD51 have an influence on cells and that TK promoter-expressed EGFP-RAD51 has a cellular characteristic comparable to endogenous RAD51 suggesting that this expression construct be an excellent tool for live-cell imaging approaches to study RAD51.

CONCLUSION

Together with the quantification of endogenous RAD51 in human cells under multiple conditions we provide tools and parameters for the quantitative understanding and modeling of cellular processes.

MATERIALS AND METHODS

Cell culture, chromatin fractionation, and DNA damage induction

The human keratinocyte cell line HaCaT, breast adenocarcinoma cell line MCF7, HCT-116 colon carcinoma cells, HeLa cervical adenocarcinoma cells, hepatocellular carcinoma cell line Hep2G, and U2OS osteosarcoma cells as well as primary human fibroblasts BJ (skin) and Wi38 (lung) [18] were cultured in DMEM supplemented with 10% fetal calf serum (FCS). Cells were grown to 80% confluence and were passaged at a split in ratio of 1:5. Cells were harvested at 70-90% confluence and cell numbers were determined by a Neubauer counting chamber. Afterwards, cells were lysed in a buffer containing 100 mM sodium phosphate pH 7.5, 5 mM EDTA, 2 mM $MgCl_2$, 0.1% CHAPS, 500 µM leupeptine, and 0.1 mM PMSF, and sonicated. After centrifugation (15 min; 15000 rpm), 5x loading buffer was added to the supernatants, the solution was incubated for 10 min at 98°C. Proteins were immediately processed further for immunoblotting or stored until further analysis at -20 °C.

For chromatin preparation, cells were processed as described [29]. Briefly, U2OS cells were resuspended in buffer N (15 mM Tris/HCl pH 7.5, 60 mM KCl, 15 mM NaCl, 5 mM $MgCl_2$, 1 mM $CaCl_2$, 2 mM Na-vanadate, 250 mM sucrose, 1 mM DTT, 2.5 µg/ml leupeptin, 1 mM PMSF, 0.3% NP-40) and incubated on ice for 5 min to lyse cell membrane followed by centrifugation (2000 rpm, 5 min, 4 °C) to sediment nuclei. The supernatant contained the cytosolic fraction of cells. The nuclei were washed three times using buffer N without NP-40. Afterwards, nuclei were resuspended and lysed by nuclei-lysis-buffer containing PIPES pH 6.5, 10 mM EDTA, 2.5 µg/ml protease inhibitor cocktail, and 1 mM PMSF on ice for 10 min. Lysed nuclei were centrifuged (6000 rpm, 20 min, 4 °C) to collect the chromatin fraction and to separate it from the nucleoplasmic extract. The chromatin pellet was washed once in nuclei-lysis-buffer, centrifuged (6000 rpm, 10 min, 4 °C), and proteins were solubilized in SDS loading buffer.

DNA damage was induced by treating cells with 12.5 µg/ml bleomycin for 30 min. After the incubation, medium was exchanged and cells were harvested after different time points. When DNA damage was induced by γ-irradiation, cells were treated with 5 Gy by exposure to ^{137}Cs source followed by a 5 h incubation to allow DNA repair processes to take place.

Cell cycle analysis

Cells were fixed in 70% ethanol (3h; -20°C). Subsequently, cells were stained with a solution containing 50 µg/ml propidium iodide, 50 µg/mL RNase A and 0,05%Triton X-100. Cells were analyzed with the LSR II flow cytometer (BD) and FlowJo (Tree Star Inc, Ashland, Oregon).

Western blotting and Antibodies

RAD51 was examined in crude cell extracts of human cell lines and in the chromatin fraction of U2OS cells. Proteins derived from untreated cells (control) and cells treated with bleomycin or γ-irradiation were quantitatively analyzed by western blotting using anti-RAD51 rabbit polyclonal antibody (sc-8349; Santa Cruz) at 1:200 or anti-RAD51 mouse monoclonal antibody (sc-377467; Santa Cruz) at 1:1000. Western blot bands were recorded by Gbox Chemi 16 Bio Imaging System (Syngene) and densiometrically analyzed using ImageJ.

Anti-RAD51 rabbit polyclonal antibody (ABE257; Millipore) at 1:250 was used in immunofluorescence staining as primary antibody which were detected with species-specific secondary antibody linked to fluorescein, (Dianova) at 1:200.

Plasmid constructions

A TK-EGFP plasmid [27] was treated with *Nhe*I and *Ase*I restriction enzymes to receive the HSV-TK promotor sequence. Afterwards, the HSV-TK promotor sequence was cloned between the *Nhe*I and *Ase*I restriction sites in an EGFP-RAD51 vector thereby excluding its CMV promotor sequence. The correct insertion of the PCR product in the distinct vector was confirmed by DNA sequencing.

Immunocytochemistry and confocal microscopy

Cells grown on coverslips were fixed with 4% *para*-formaldehyde for 10 min at room temperature. Immunofluorescence was performed as previously described [23]. Samples were scanned with a Zeiss LSM 510 laser scanning confocal device attached to an Axioplan 2 microscope using a 63x Plan-Apochromat oil objective (Carl Zeiss, Jena, Germany). Fluorescein dye was excited by laser light at 488. DNA was detected using DAPI (4,6-diamidino-2-phenylindole) and 406 nm laser excitation. Single optical sections were selected either from manual scans, or taken from stack projections. Images were merged using the LSM 510 (Carl Zeiss, Jena, Germany) software and stored as TIFF files. Figures were assembled from the TIFF files using Adobe Photoshop software.

Statistical analysis

Each experiment was repeated at least three times unless stated otherwise. Data are presented as the mean ±SD. Statistical comparisons were performed using paired two-tailed Student's *t* test. A *P* value of < 0.05 was considered statistically significant.

ACKNOWLEDGEMENTS

We are grateful to Drs Peter Hemmerich for primary human fibroblasts and Shamci Monajembashi for assistance at the γ-irradiation source.

REFERNCES

(1) Milo R, Jorgensen P, Moran U, Weber G. Springer M. BioNumbers – the database of key numbers in molecular and cellular biology. Nucleic Acids Res 2010;38:D750-753.

(2) Chapman JR, Taylor MRG, Boulton SJ. Playing the end game: DNA double-strand repair pathway choise. Mol Cell 2012;47:497-510.

(3) Lisby M, Rothstein R. Cell biology of mitotic recombination. Cold Spring Harb Perspect Biol 2015;7:a016235.

(4) Wright WD, Shah SS, Heyer WD. Homologous recombination and the repair of DNA double-strand breaks. J Biol Chem 2018;293:10524-10535.

(5) Essers J, Houtsmuller AB, van Veelen L, Paulusma C, Nigg AL, Pastnik A, Vermeulen W, Hoeijmakers JHJ, Kanaar R. Nuclear dynamics of RAD52 group homologous recombination proteins in response to DNA damage. EMBO J 2002;21:2030-2037.

(6) Otterlei M, Bruheim P, Ahn B, Bussen W, Karmakar P, Baynton K, Bohr VA. Werner syndrome protein participates in a complex with RAD51, RAD54, RAD54B and ATR in response to ICL-induced replication arrest. J Cell Sci 2006;119:5137-5146.

(7) Bekker-Jensen S, Lukas C, Kitagawa R, Melander F, Kastan MB, Bartek J, Lukas J. Spatial organization of the mammalian genome surveillance machinery in response to DNA strand breaks. J Cell Biol 2006;173:195-206.

(8) Burgreev DV, Rossi MJ, Mazin AV. Cooperation of RAD51 and RAD54 in regression of a model replication fork. Nucleic Acids Res 2011;39:2153-2164.

(9) Wright WD, Heyer WD. Rad54 functions as a heteroduplex DNA pump modulated by its DNA substrates and Rad51 during D-loop formation. Mol Cell 2014; 53: 420-432.

(10) Qi Z, Redding S, Lee JY, Gibb B, Kwon Y, Niu H, Gaines WA, Sung P, Greene EC. DNA sequences alignment by microhomology sampling during homologous recombination. Cell 2015;16:1-14.

(11) Foertsch F, Szambowska A, Weise A, Zielinski A, Schlott B, Kraft F, Mrasek K, Borgmann K, Pospiech H, Grosse F, Melle C. S100A11 plays a role in homologous recombination and genome maintenance by influencing the persistence of RAD51 in DNA repair foci. Cell Cycle 2016;15:2766-2779.

(12) Abeyta A, Castella M, Jacquemont C, Taniguchi T. NEK8 regulates DNA damage-induced RAD51 foci formation and replication fork protection. Cell Cycle 2017;16:335-347.

(13) Ito K, Murayama Y, Takahashi M, Iwasaki H. Two three-strand intermediates are processed during Rad51-driven DNA strand exchange. Nat Struct Mol Biol 2018;25:29-36.

(14) Whelan DR, Lee WTC, Yin Y, Ofri DM, Bermudez-Hernandez K, Keegan S, Fenyo D, Rothenberg E. Spatiotemporal dynamics of homologous recombination repair at single collapsed replication forks. Nat Commun 2018;9:3882.

(15) Lisby M, Mortensen UH, Rothstein R. Colocalization of multiple DNA double-strand breaks at a single Rad52 repair centre. Nat Cell Biol 2003;5:572-577.

(16) Takai KK, Kibe T, Donigian JR, Frescas D, de Lange T. Telomere protection by TTP1/POT1 requires tethering to TIN2. Mol Cell 2011;44:647-659.

(17) Braet C, Stephan H, Dobbie IM, Togashi DM, Ryder AG, Foldes-Papp Z, Lowndes N, Nasheuer HP. Mobility and distribution of replication protein A in living cells using fluorescence correlation spectroscopy. Exp Mol Pathol 2007;82: 156-162.

(18) Klement K, Melle C, Murzik M, Diekmann S, Norgauer J, Hemmerich P. Accumulation of annexin A5 at the nuclear envelope is a biomarker of cellular aging. Mech Ageing Dev 2012;133:508-522.

(19) Moran U, Phillips R, Milo R. SnapShot: Key numbers in biology. Cell 2010;141:1262-1262e1.

(20) Bhat KP, Cortez D. RPA and RAD51: fork reversal, fork protection, and genome stability. Nat Struct Mol Biol 2018,25:446-453.

(21) West SC, Blanco MG, Chan YW, Matos J, Srbajna S, Wyatt HDM. Resolution of recombination intermediates: Mechanisms and regulation. Cold Spring Harb Symp Quant Biol 2015;80:103-109.

(22) Chung WH, Zhu Z, Papusha A, Malkova A, Ira G. Defective resection at DNA double-strand breaks leads to de novo telomere formation and enhances gene targeting. PLoS Genet 2010;6:e1000948.

(23) Murzik U, Hemmerich P, Weidtkamp-Peters S, Ulbricht T, Bussen W, Hentschel J, von Eggeling F, Melle C. Rad54B targeting to DNA double-strand break repair sites requires complex formation with S100A11. Mol Biol Cell 2008;19:2926-2935.

(24) Chen F, Nastasi A, Shen Z, Brenneman M, Crissman H, Chen DJ. Cell cycle-dependent protein expression of mammalian homologs of yeast DNA double-strand break repair genes Rad51 and Rad52. Mutat Res 1997;384:205-211.

(25) Lisby M, Barlow JH, Burgess RC, Rothestein R. Choreography of the DNA damage response: Spatiotemporal relationships among checkpoint and repair proteins. Cell 2004;118:699-713.

(26) Mazin AV, Mazina OM, Bugreev DV, Rossi MJ. Rad54, the motor of homologous recombination. DNA repair 2010;9:286-302.

(27) Ali R, Ramadurai S, Barry F, Nasheuer HP. Optimizing fluorescent protein expression for quantitative fluorescence microscopy and spectroscopy using herpes simplex thymidine kinase promotor sequences. FEBS Open Bio 2018;8:1043-1060.

(28) Flygare J, Fält S, Ottervald J, Castro J, Dackland AL, Hellgren, Wennborg A. Effects of HsRad51 overexpression on cell proliferation, cell cycle progression, and apoptosis. Exp Cell Res (2001); 268; 61-69.

(29) Remboutsika E, Lutz Y, Ganzmuller A, Vonesch JL, Losson R, Chambon P. The putative nuclear mediator TIF1alpha is highly associated with euchromatin. J Cell Sci 1999;112:1671-1683.

FIGURE LEGENDS

Figure 1. Determination of the number of RAD51 molecules in human cell lines. (A) Coomassie Brilliant blue-stained gel of purified RAD51 (1.35 pmol) to show the quality of the purified recombinant protein. [M = protein weight marker]. (B-I) Western blots of whole cell extracts (n = 3) are presented. The proteins were derived from (B) HeLa (cervical adenocarcinoma; lane 1 to 3: 3.31x, 2.92x, and $3.05x10^6$ cells), (C) HepG2 (hepatocellular carcinoma; lane 1 to 3: 3.34x, 1.8x, and $1.94x10^6$ cells), (D) U2OS (osteosarcoma; lane 1 to 3: 1.1x, 0.98x, and $1.58x10^6$ cells), (E) MCF7 (breast adenocarcinoma; lane 1 to 3: 1.36x, 1.82x, and $1.64x10^6$ cells), (F) HaCaT (keratinocytes; lane 1 to 3: 1.29x, 1.64x, and $1.33x10^6$ cells), (G) HCT116 (colon carcinoma; lane 1 to 3: 2.37x, 1.02x, and 1.31x 10^6 cells), (H) BJ (primary skin fibroblasts; lane 1 to 3: 0.24x, 0.46x, and $1.07x10^6$ cells), and (I) Wi-38 (primary lung fibroblasts; lane 1 to 3: 0.24x, 0.18x, and $0.1x10^6$ cells) for determination of RAD51 protein numbers and subjected to western blotting using an anti-RAD51 antibody to detect the protein crude extracts. Increasing amounts of purified RAD51 (6.75, 13.5, 27, 54, 108, and 216 fmol) were loaded in parallel

on each gel and used as a standard for quantitative protein determination. (J) Table summarizing the measured average RAD51 numbers in human cells from 3 independent experiments and standard deviation values (SD) are provided.

Figure 2. The number of RAD51 molecules is unchanged by induction of DNA damage. (A) Cell extract from control HaCaT cells (1.19 x 10^6 cells, lane 1) or cells treated with bleomycin (12.5 µg/ml) for 30 min (lane 2 to 4: 1.12x, 1.1x, and 2.1 x 10^6 cells), followed by release in fresh medium (lane 2 to 5: 2.5 h, 4.5 h, and 23.5 h) were analyzed by western blotting using a specific RAD51 antibody. Purified RAD51 was loaded on the gel in parallel and used as a standard to quantitatively determine protein amounts (lane 5 to 9: 13.5 fmol, 27 fmol, 54 fmol, 108 fmol, and 216 fmol). A representative western blot is presented (n =3). The measured RAD51 molecules per cell are presented in panel at the bottom. Data shown are the average and SD value of 3 independent experiments. (B) HaCaT keratinocytes were exposed to γ-rays (5 Gy) (lane 1 to 3: 4.68x, 4.13x, and 4.2x10^6 cells) and analyzed by immunoblotting using a specific RAD51 antibody 5 h after irradiation. Purified RAD51 was used as a standard (lane 4 to 9: 6.75 fmol, 13.5 fmol, 27 fmol, 54 fmol, 108 fmol, and 216 fmol). A representative western blot is presented (n =3). Quantitative measurements of RAD51 molecules per cell derived from cells treated with γ-irradiation and results from (A) for comparison are presented in panel at the bottom. All values are the average and SD value of 3 independent experiments. (C) U2OS cells treated with bleomycin (12.5 µg/ml) for 30 min (lane 2 to 4: 0.53x, 0.52x, and 0.86x10^6 cells) or untreated cells (lane 1: 0.54x10^6 cells), followed by release in fresh medium (lane 2 to 4: 2.5 h, 4.5 h, and 23.5 h) were analyzed by western blotting using a specific RAD51 antibody. Purified RAD51 was used as a standard (lane 5 to 9: 13.5 fmol, 27 fmol, 54 fmol, 108 fmol, and 216 fmol). A representative western blot is presented (n =3). (D) The chromatin fraction of U2OS cells treated with bleomycin (12.5 µg/ml) for 30 min (lane 2 to 4: 1.1x, 1.09x, and 1.24x10^6 cells) or chromatin fraction of untreated cells (lane 1: 1.06x10^6 cells), followed by release in fresh medium (lane 2 to 4: 2.5 h, 4.5 h, and 23.5 h) were analyzed by western blotting using a specific RAD51 antibody. In parallel increasing amounts of purified RAD51 (6.75 fmol, 13.5 fmol, 27 fmol, 54 fmol, and 108 fmol) were used as a standard. A representative western blot is presented (n =3). Quantitative measurements of RAD51 molecules per cell are present in panel at the bottom and are

the average 3 independent experiments. SD values are also shown. Data were analyzed by using two-sided Student's *t* test and the significance was determined *** $P < 0.005$

Figure 3. Effects of ectopic RAD51 expression on nuclear structures and cell cycle distribution.

(A) Cells were treated with 12.5 µg/ml bleomycin for 30 min to induce DSBs and released in fresh medium for 90 min followed by immunostaining with an anti-RAD51 antibody. Afterwards, cells were analyzed by laser scanning microscopy (LSM, bars: 10 µm). The average and SD values of counted RAD51 foci are presented in the diagram on the right ($n \geq 11$ cells). (B) U2OS cells expressing CMV-EGFP-RAD51 and TK-EGFP-RAD51 (upper and lower panel, respectively) analyzed by LSM (bars: 10 µm). (C-D) Immunoblots of U2OS cell extracts expressing (C) CMV-EGFP-RAD51 (lane 1 to 3: 1.3x, 1.27x, and $0.7x10^6$ cells) or (D) TK-EGFP-RAD51 (lane 1 to 3: 0.19x, 0.36x, and $0.36x10^6$ cells). Purified RAD51 was used as a standard (panel C: lane 4 to 8: 54, 108, 216, 337.5, and 675 [fmol]; panel D: lane 4 to 8: 13.5, 27, 54, 108, and 216 [fmol]). (E) Cell cycle phase distributions of U2OS cells expressing CMV-EGFP, CMV-EGFP-RAD51, TK-EGFP or TK-EGFP-RAD51 as well as control U2OS cells were determined by FACS. The average ($n = 3$) and SD values are presented. Data were analyzed by using two-sided Student's *t* test and the significance was determined * $P < 0.05$, ** $P < 0.01$.

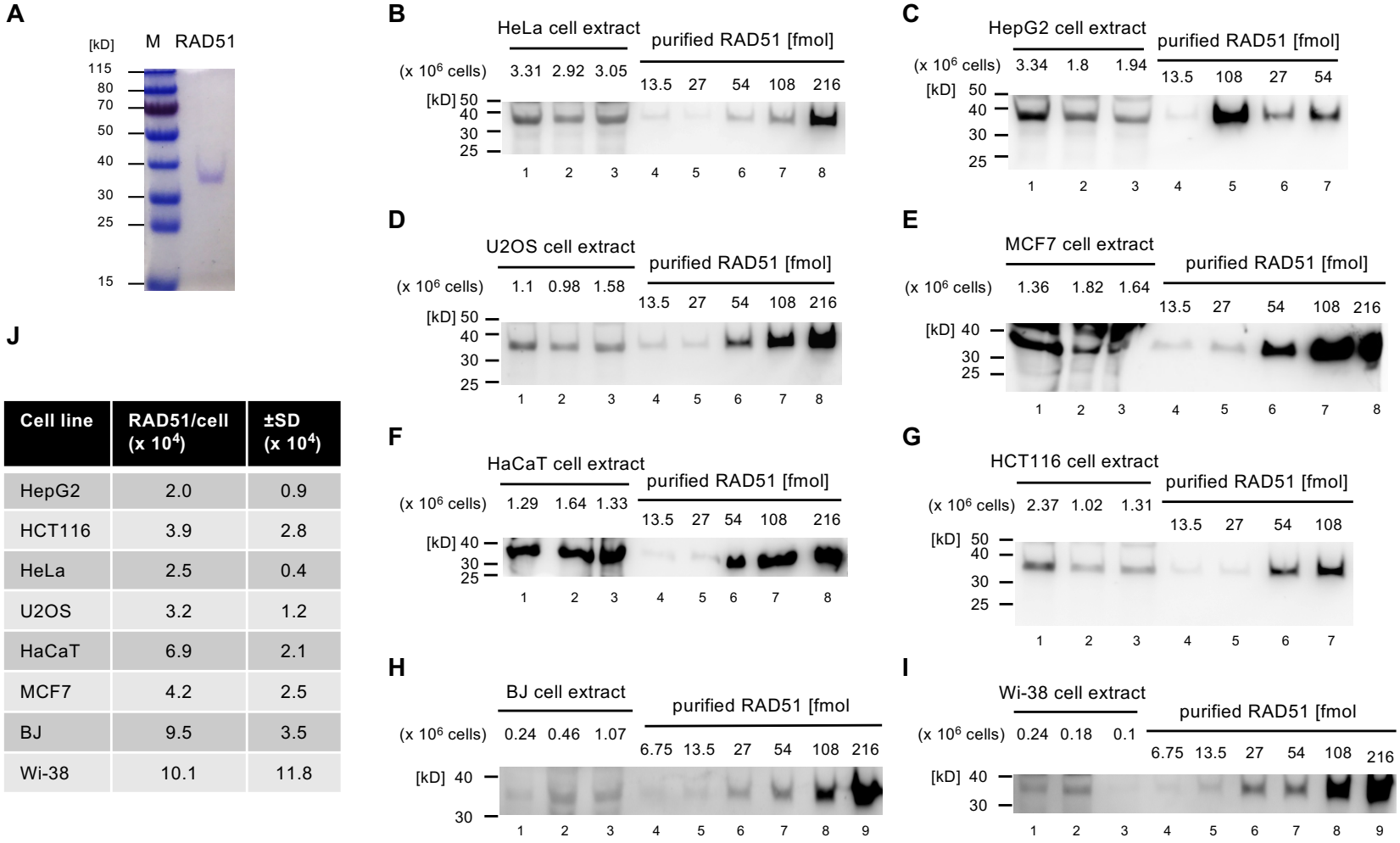

J

Cell line	RAD51/cell (x 10^4)	±SD (x 10^4)
HepG2	2.0	0.9
HCT116	3.9	2.8
HeLa	2.5	0.4
U2OS	3.2	1.2
HaCaT	6.9	2.1
MCF7	4.2	2.5
BJ	9.5	3.5
Wi-38	10.1	11.8

Fig. 1

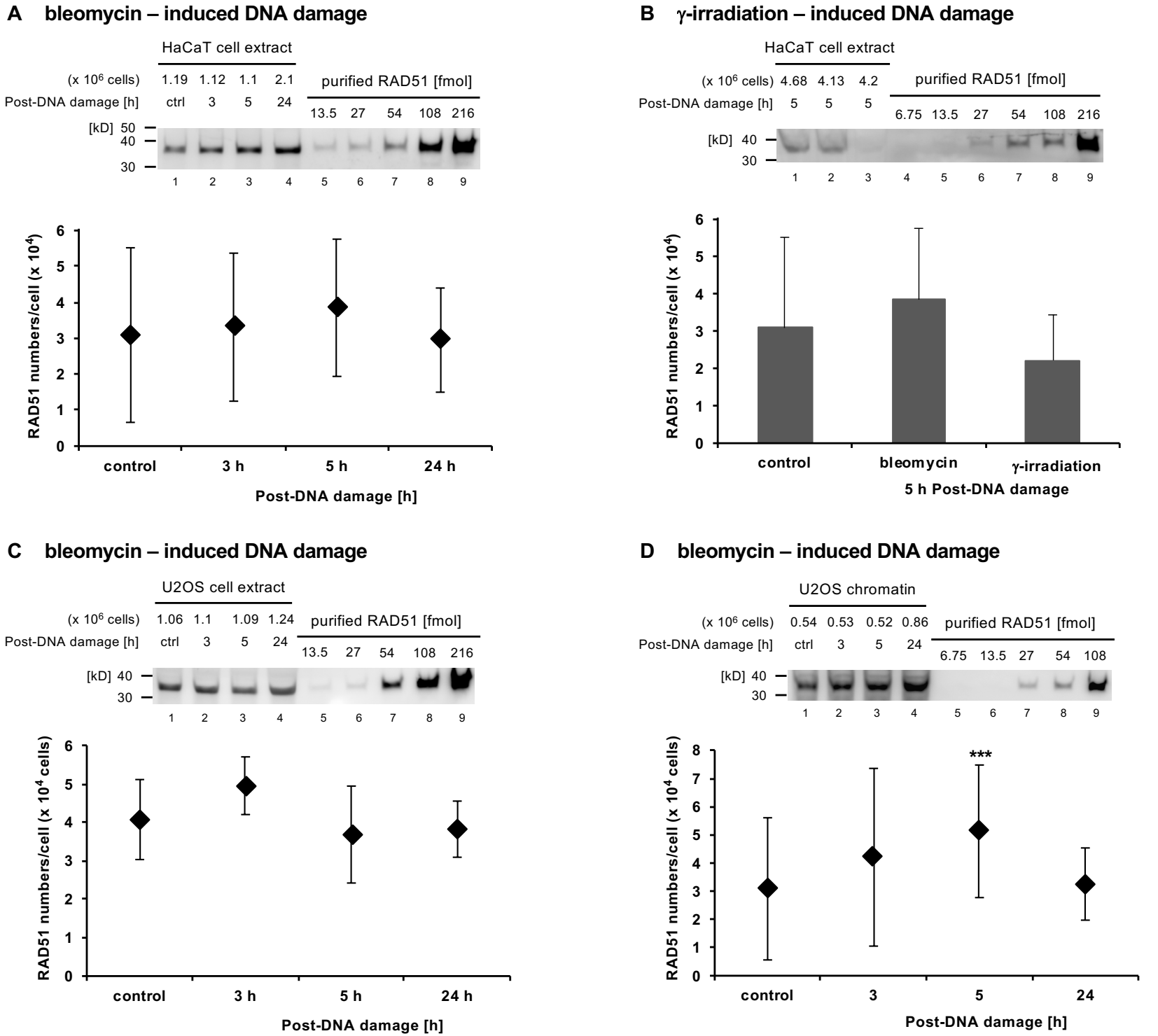
A bleomycin – induced DNA damage
HaCaT cell extract
(x 10^6 cells) 1.19 1.12 1.1 2.1
purified RAD51 [fmol]
Post-DNA damage [h] ctrl 3 5 24
13.5 27 54 108 216
[kD] 50 40 30
1 2 3 4 5 6 7 8 9
RAD51 numbers/cell (x 10^4)
control 3 h 5 h 24 h
Post-DNA damage [h]
B γ-irradiation – induced DNA damage
HaCaT cell extract
(x 10^6 cells) 4.68 4.13 4.2
purified RAD51 [fmol]
Post-DNA damage [h] 5 5 5
6.75 13.5 27 54 108 216
[kD] 40 30
1 2 3 4 5 6 7 8 9
RAD51 numbers/cell (x 10^4)
control bleomycin γ-irradiation
5 h Post-DNA damage
C bleomycin – induced DNA damage
U2OS cell extract
(x 10^6 cells) 1.06 1.1 1.09 1.24
purified RAD51 [fmol]
Post-DNA damage [h] ctrl 3 5 24
13.5 27 54 108 216
[kD] 40 30
1 2 3 4 5 6 7 8 9
RAD51 numbers/cell (x 10^4 cells)
control 3 h 5 h 24 h
Post-DNA damage [h]
D bleomycin – induced DNA damage
U2OS chromatin
(x 10^6 cells) 0.54 0.53 0.52 0.86
purified RAD51 [fmol]
Post-DNA damage [h] ctrl 3 5 24
6.75 13.5 27 54 108
[kD] 40 30
1 2 3 4 5 6 7 8 9
***
RAD51 numbers/cell (x 10^4 cells)
control 3 5 24
Post-DNA damage [h]

Fig. 2

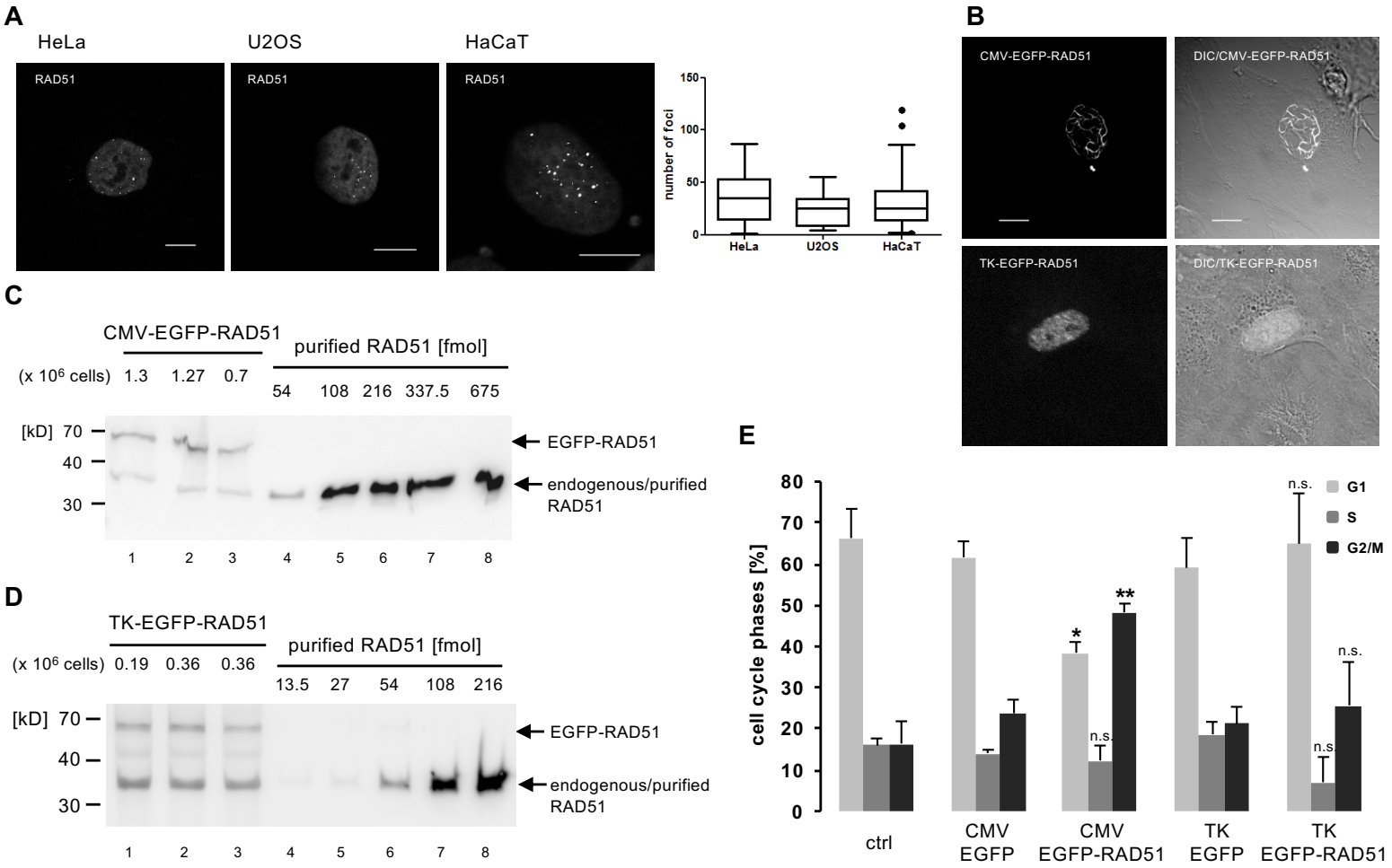
A
HeLa
U2OS
HaCaT
RAD51
RAD51
RAD51
number of foci
150
100
50
0
HeLa
U2OS
HaCaT
B
CMV-EGFP-RAD51
DIC/CMV-EGFP-RAD51
TK-EGFP-RAD51
DIC/TK-EGFP-RAD51
C
CMV-EGFP-RAD51
purified RAD51 [fmol]
(x 10^6 cells) 1.3 1.27 0.7
54 108 216 337.5 675
[kD] 70
40
30
EGFP-RAD51
endogenous/purified RAD51
1 2 3 4 5 6 7 8
D
TK-EGFP-RAD51
purified RAD51 [fmol]
(x 10^6 cells) 0.19 0.36 0.36
13.5 27 54 108 216
[kD] 70
40
30
EGFP-RAD51
endogenous/purified RAD51
1 2 3 4 5 6 7 8
E
cell cycle phases [%]
80
70
60
50
40
30
20
10
0
G1
S
G2/M
n.s.
n.s.
n.s.
*
**
n.s.
ctrl
CMV EGFP
CMV EGFP-RAD51
TK EGFP
TK EGFP-RAD51

Fig. 3